Review of Scientific Instruments

A combined rotating disk electrode–surface x-ray diffraction setup for surface structure characterization in electrocatalysis

Cite as: Rev. Sci. Instrum. **93**, 065111 (2022); https://doi.org/10.1063/5.0087864
Submitted: 10 February 2022 • Accepted: 22 May 2022 • Published Online: 22 June 2022

Leon Jacobse, Ralf Schuster, Johannes Pfrommer, et al.

Review of Scientific Instruments ARTICLE scitation.org/journal/rsi

A combined rotating disk electrode–surface x-ray diffraction setup for surface structure characterization in electrocatalysis

Cite as: Rev. Sci. Instrum. 93, 065111 (2022); doi: 10.1063/5.0087864
Submitted: 10 February 2022 • Accepted: 22 May 2022 •
Published Online: 22 June 2022

Leon Jacobse,[1,a] Ralf Schuster,[2] Johannes Pfrommer,[1,3] Xin Deng,[1,2] Silvan Dolling,[4] Tim Weber,[3] Olof Gutowski,[5] Ann-Christin Dippel,[5] Olaf Brummel,[2] Yaroslava Lykhach,[2] Herbert Over,[3] Jörg Libuda,[2] Vedran Vonk,[1] and Andreas Stierle[1,4]

AFFILIATIONS

[1] Centre for X-ray and Nano Science CXNS, Deutsches Elektronen-Synchrotron DESY, Notkestr. 85, 22607 Hamburg, Germany
[2] Interface Research and Catalysis, Erlangen Center for Interface Research and Catalysis, Friedrich-Alexander-Universität Erlangen-Nürnberg, Egerlandstraße 3, 91058 Erlangen, Germany
[3] Institute of Physical Chemistry and Center for Materials Research, Justus Liebig Universität Gießen, Heinrich-Buff-Ring 17, 35392 Gießen, Germany
[4] Fachbereich Physik, Universität Hamburg, Jungiusstrasse 11, 20355 Hamburg, Germany
[5] Deutsches Elektronen-Synchrotron DESY, Notkestr. 85, 22607 Hamburg, Germany

[a] **Author to whom correspondence should be addressed:** leon.jacobse@desy.de

ABSTRACT

Characterizing electrode surface structures under operando conditions is essential for fully understanding structure–activity relationships in electrocatalysis. Here, we combine in a single experiment high-energy surface x-ray diffraction as a characterizing technique with a rotating disk electrode to provide steady state kinetics under electrocatalytic conditions. Using Pt(111) and Pt(100) model electrodes, we show that full crystal truncation rod measurements are readily possible up to rotation rates of 1200 rpm. Furthermore, we discuss possibilities for both potentiostatic as well as potentiodynamic measurements, demonstrating the versatility of this technique. These different modes of operation, combined with the relatively simple experimental setup, make the combined rotating disk electrode–surface x-ray diffraction experiment a powerful technique for studying surface structures under operando electrocatalytic conditions.

I. INTRODUCTION

Understanding electrocatalytic processes at an atomic level is essential to develop the most efficient electrocatalysts.[1] To study structure–activity relationships, typical approaches make use of model catalysts that have the same atomic surface structure on a macroscopic scale, i.e., single crystal electrodes. Alternatively, techniques with a high spatial resolution cannot only be applied on such model electrodes but also on heterogeneous samples, e.g., polycrystalline materials or supported nanoparticles. However, these studies mostly assume that the surface structure is not affected by the electrochemical environment, as it is determined (if at all) in a separate experiment. The reason for this is that it is experimentally challenging to directly measure atomically resolved surface structures under *in situ* or even operando conditions.

Surface x-ray diffraction (SXRD) has proven to be a powerful technique for structural characterization experiments and its applicability in electrochemistry has been boosted strongly by the development of high-energy (20–100 keV, HE-SXRD) beamlines and large two-dimensional (2D) detectors.[2–4] As a result, the time needed for the measurement has decreased drastically, from hours to minutes, while also unwanted, photo(electro)chemical, side-reactions are damped. In practice, this means that the only movement necessary for crystal truncation rod (CTR) measurements is an in-plane

sample rotation.[5] As reviewed recently by Harlow *et al.*, HE-SXRD has been used in electrochemistry to study, e.g., reconstruction and oxidation processes as a function of the applied potential.[3] Although this development is a huge improvement compared to *ex situ* experiments, eventually one would like to observe structures while an electrocatalytic reaction occurs, i.e., under operando conditions. From an electrochemical point of view, such experiments are not trivial as mass transport forms a large barrier for studying the macroscopically sized model electrodes under high current densities. Under static conditions, the activity is often limited by the diffusion of reactants (products) to (from) the surface, which is a time-dependent process,[6]

$$j_{\mathrm{lim}} = \frac{nF\sqrt{D}C}{\sqrt{\pi t}}, \tag{1}$$

where j_{lim} is the diffusion-limited current density, n is the number of electrons involved in the reaction, F is the Faraday constant, D and C are the diffusion constant and concentration of the (limiting) species in the bulk solution, and t is the time. Previously, operando HE-SXRD experiments were performed utilizing a constant flow of electrolytes to increase the rate of the mass transport through the electrolyte solution.[7–11] Although this approach results in a steady-state condition, the flow conditions in the used cell, whose geometry is optimized for the x-ray experiment,[12] remain largely unknown.

A standard way in electrocatalysis to control mass transport in a reproducible manner is the rotating disk electrode (RDE) technique.[6] In an RDE experiment, the sample electrode rotates fast (100–10.000 rpm) around the surface normal, which induces convection in the electrolyte and leads to a diffusion layer thickness (δ) and j_{lim} that depend on the RDE rotation rate,[6]

$$\delta = 1.61\nu^{1/6}\omega^{-1/2}D^{1/3}, \tag{2}$$

$$j_{\mathrm{lim}} = 0.62nFD^{2/3}\nu^{-1/6}C\omega^{1/2}, \tag{3}$$

where ν is the viscosity of the electrolyte and ω is the RDE rotation rate. Not only is the diffusion-limited current obtained in an RDE experiment much larger than under static conditions, but as j_{lim} is now no longer time-dependent it enables experiments under steady state conditions.

As both HE-SXRD and RDE experiments rely on a rotation of the sample around the surface normal, this provides an ideal opportunity for structural characterization experiments under operando conditions. Here, we describe the development of a setup for such simultaneous experiments and showcase several modes of operation in which the data can be collected. The used model system is the oxygen reduction on Pt(111) and Pt(100) and their surface oxidation. The detailed results from these experiments, including quantitative structural analysis, will be discussed in a separate study. Focusing on the experimental technique, the examples shown here demonstrate that the combination of HE-SXRD with the RDE technique is a powerful tool to study electrode surface structures under electrocatalytic conditions that cannot be obtained in a static experiment.

II. METHODS

The setup for combined RDE and SXRD experiments (see Fig. 1) is custom built and is compatible with heavy-duty synchrotron diffractometers, specifically those available at the P07 and P21.2 PETRA III beamlines at the Deutsches Elektronen Synchrotron (DESY). The main part of the RDE setup is the rigid stainless steel frame construction, onto which both the rotator and the electrochemical cell are mounted. The electrochemical cell is made from glass and is open at the top, such that the experiment can be performed in the hanging meniscus geometry. The commercial RDE (RDE-2 and MCUR control unit, Metrohm) is mounted in the upper part of the setup using a custom sample holder. Prealignment such that the surface normal is parallel to the RDE axis has to

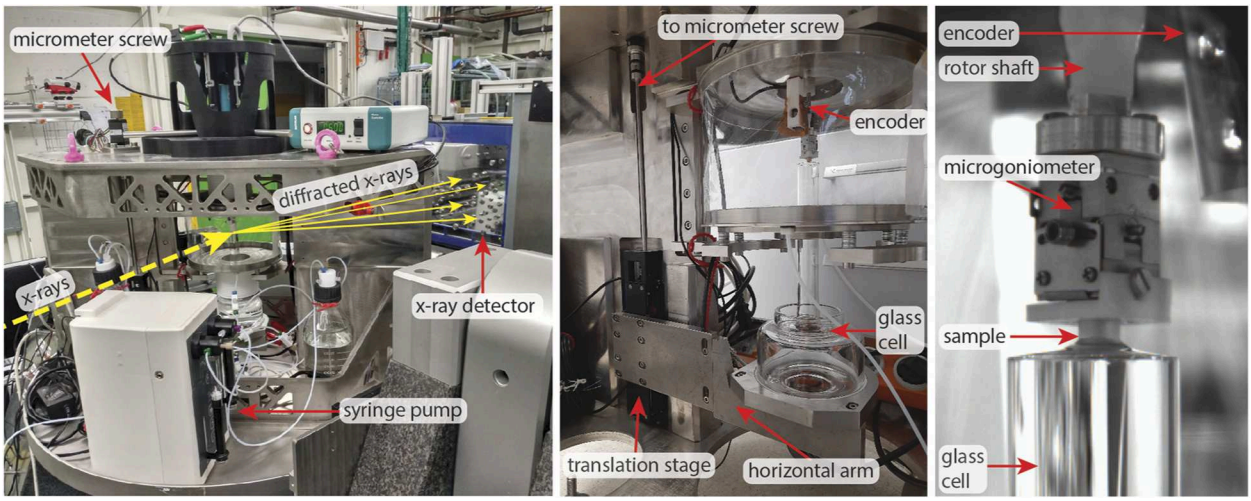

FIG. 1. Experimental setup: photographs of the entire setup as mounted at the P07 beamline (left), an overview of the construction to move the cell height (middle), and a zoomed-in view on the sample mounting (right). Note that the sample is facing downward and the diffraction pattern, thus, appears below the sample surface horizon.

be performed manually and is realized by minimizing the rotation cone from a laser reflected from the dry surface. A manual operated microgoniometer (NDN-7S4 Kohzu Precision) was added to the sample holder for the Pt(100) experiments (see Fig. 1), which made this procedure faster and more reproducible. The microgoniometer has an advertised accuracy of 0.1°, but we found our laser alignment to work well down to about 0.02° over a full rotation. Subsequently, the entire RDE assembly is aligned parallel to the diffractometer theta axis. In this way, the diffractometer angle used for defining the angle of incidence can be used. The electrochemical cell is supported from underneath by a horizontal arm, which is mounted on a linear translation stage (see Fig. 1). This allows for the vertical positioning of the cell, and thus its height relative to the beam, to be adjusted using a micrometer screw. In combination with control of the electrolyte volume using a syringe pump, this enables full control of the electrolyte meniscus without changing the sample position. The meniscus was made such that the x rays only penetrate the electrolyte and not the glass cell. A potentiostat (PGSTAT204, Metrohm) was used to control the potentials and collect the electrochemical data.

Diffraction patterns recorded with 2D detectors typically involve the rotation of the sample over a single rotation axis, which assures that different parts of reciprocal space are rotated through the Ewald sphere and are brought into diffraction condition. Since a peak is in diffraction condition only for a small fraction of the total rotation about this axis, data are taken by exposing only over a fraction of a full rotation before reading out a detector image. This gives a better signal-to-noise ratio, because less background is collected, and avoids having peak overlap. The optimum rotation range depends on the mosaicity of the sample and the number of distinguishable peaks obtained per image. In the case of SXRD, where the diffraction signals of interest are lines (CTRs), a similar situation arises. A single CTR, measured with high-energy x rays, is typically swept through the Ewald sphere by rotating the sample a few degrees around its surface normal. To assure a good signal-to-noise ratio, the detector should thus be exposed only during the time that the sample is rotating through the angular range for the CTR, possibly even a fraction of that and, thus, recording more than one detector image per CTR.

Here, we make use of the gating capabilities of the detector in combination with an encoder signal, which is activated for a single angular position of the rotator axis. Using a programmable delay and exposure time from the moment that the encoder is activated allows us to obtain a diffraction pattern from a specific angular range of the rotator axis (see Fig. 2 for a schematic view of the signals involved). This directly translates to the measurement of a particular CTR and the range in L over which it is recorded.[4] The total number of photons collected in a single detector image measured in this way may be too low to give statistically relevant data, and therefore, the measurement over the same angular range is repeated a number of times, in a similar way as pump–probe data are collected.[13]

A complicating factor in the above-mentioned scheme is a fluctuating rotator speed, which may cause ill-defined angular ranges over which the detector is exposed in case fixed delay and exposure times are used. This problem has been solved in the following way: the detector gate signals were generated using a so-called Raspberry Pi Logic Controller (PiLC), which is a field-programmable

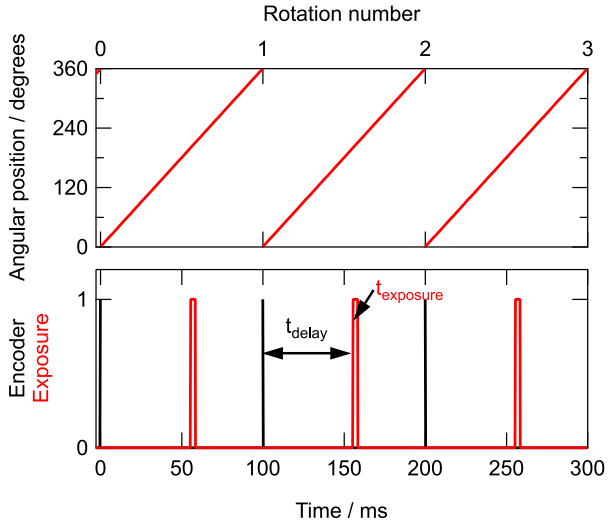

FIG. 2. Experiment scheme: a schematic overview of the method for triggering the x-ray detector using a rotation rate of 600 rpm, a delay time of 60 ms (216°), and an exposure time of 3 ms (11°) per rotation. Note that, in practice, due to small fluctuations in the rotator speed, the delay and exposure times also exhibit small fluctuations during the sequence of rotations.

gate array-based unit developed at DESY.[14] This controller was programmed to keep track of the temporal rotation speed by measuring the time between the activation of consecutive encoder signals, which is found to fluctuate over the course of an entire measurement. The angular start and end positions of the rotator during which the detector is exposed in a particular revolution are then determined from the measured rotation speed from the previous revolution. With this approach, we manage to bring the error in the azimuthal angular position (assuming a constant rotation speed within a single rotation) down to 0.01–0.3°, depending on the rotation speed. Clearly, this scheme works very well and enables our experiments, despite the relatively low accuracy of commercially available RDE systems (typically 1% or 1 rpm).

The HE-SXRD experiments were performed at the second experimental hutch (EH2) at beamline P07 at PETRA III, DESY,[15] employing photon energy of 74.8 keV. The incidence angle was set at 0.03°, close to the critical angle of total external reflection for Pt. Diffraction patterns were recorded with a high-energy 2D area detector (Pilatus3X CdTe 2M, Dectris), with a total sensitive area of 253.7 × 288.8 mm^2 and a pixel size of 172 × 172 μm^2, which was placed at a distance of 800 mm from the sample.

In a typical HE-SXRD experiment, one would record a large number of images within the selected angular range to optimize the signal-to-noise ratio. However, at the maximum (continuous) detector frequency (250 Hz) and a typical RDE rotation rate of 600 rpm, the integration window is already 14.4°. Electronic gating of the detector (down to exposure times of 200 ns) could be used to obtain similar angular resolution compared to conventional experiments. However, the readout frequency is still maximum 250 Hz, and the experimental time has to be increased to measure sufficient data at all angles. Not only would this lead to large, unsorted, datasets

(~2.5 GB/s with a typical measurement time, without electronic gating, of 10 min), but the analysis is further complicated because the RDE does not provide an absolute positioning method such that the data collection is not necessarily linearly distributed across the angular range. Using the electronic gating to measure a single CTR within a typical angular window of 10°, obtaining images every 0.1° and a total exposure time of 0.1 s for each image, would result in a measurement time of 10 h and a dataset of 3.6 TB, while possibly suffering from the accuracy of the determination of the azimuthal angle. In the future, faster detector readout and possibly multiple internal detector buffers will drastically increase the feasibility of such scans. As an initial solution, we employ a much simpler method of using the internal summing of the detector images for a predetermined number of RDE rotations. The electronic gating is triggered by the rotary encoder that is mounted on the shaft of the RDE. This procedure results in a single detector image for each selected angular range. Our approach somewhat compromises the signal-to-noise ratio and limits the possibilities for background correction. However, we demonstrate here that, for strong scatterers like Pt, this is not a problem and quantitative CTR integration remains possible. To construct in-plane reciprocal space maps, our method can be combined with traditional angular scans.

All glassware and other parts of the setup that came into contact with the electrolyte were soaked for at least 24 h in a 1 g/l $KMnO_4$/0.5 M H_2SO_4 solution. Subsequently, the syringes and tubing of the syringe pump were flushed extensively with hot ultrapure water (>18.2 $M\Omega$ cm). All other parts were boiled at least five times in ultrapure water. The hat-shaped Pt(111) sample (cut and polished <0.1°, MaTeck) is prepared by flame annealing (5 min at ~1250 K) and cooling in a reducing atmosphere (1:4 H_2/Ar mixture). After cooling down, bromine adsorption (by dipping the sample in a 0.1 mM NaBr solution) was used to protect the surface against contamination during the prealignment (performed in air).[16] After establishing the contact with the electrolyte under potential control, the bromine was stripped by potential cycling into the hydrogen adsorption region. The Pt(100) electrode (cut and polished <0.1°, MaTeck) is prepared by flame-annealing and cooling down in Ar. High-purity perchloric acid (99.999% trace metals basis, Sigma-Aldrich) is used to prepare the 0.1 M $HClO_4$ electrolyte solution. Several hours prior to and during the experiment, the electrolyte is purged with Ar or O_2. The experiment was performed in a three-electrode configuration using a miniature reversible hydrogen electrode (RHE, gaskatel) as a reference electrode and a coiled platinum wire (99.999%, MaTeck) as the counter electrode.

III. RESULTS AND DISCUSSION

A. Potentiostatic measurements

Figure 3(a) shows a section of the x-ray detector images as a function of the rotation rate, cropped to show only the (1 1) CTR. These measurements were performed at a sample potential of 0.6 V vs RHE in 0.1 M $HClO_4$. The number of rotations per image was scaled such that the total experimental time was 100 s in all cases (e.g., 500 rotations at 300 rpm and 3000 rotations at 1800 rpm). Note that, as illustrated in Fig. 2, the exposure time is only a fraction of the total experimental time. Here, an angular range of 8° (out of the full 360°) was selected, leading to a total exposure time of 2.22 s per experiment. Although the CTR signal (weak vertical line) can be clearly identified in the different images, the different measurements differ clearly. With increasing rotation rate, most notably at 1800 rpm, powder rings appear in the diffraction pattern. Simultaneously, an increasing diffuse background is observed around the

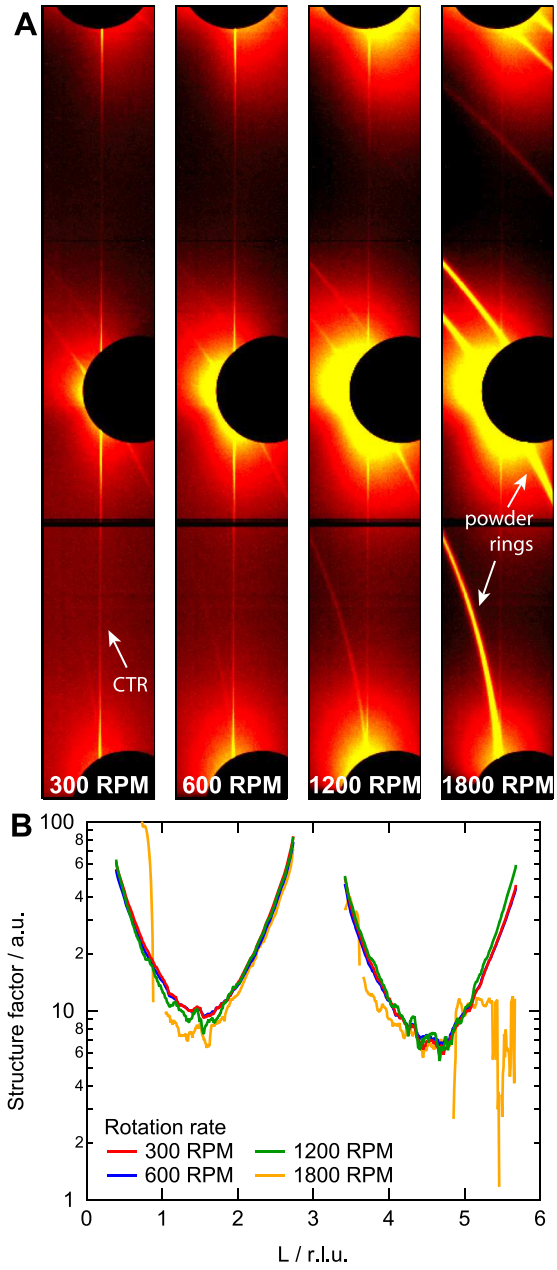

FIG. 3. Effect of rotation rate: (a) crops of the detector images showing the (1 1) CTR measured at 0.6 V vs RHE as a function of the rotation rate, from left to right, 300, 600, 1200, and 1800 rpm, respectively. The color scale is the same in all images. Note that the images are mirrored with respect to the real orientation, i.e., the largest L values are at the top of the image. (b) Structure factors determined from the images shown in (a).

Bragg peaks (which are blocked by the black circular beamstops). It is important to realize that the appearance of the powder rings is not related to a changing surface structure, as that is expected to remain unaffected by the rotation alone and the rings also disappear again upon decreasing the rotation rate. Instead, it seems more likely that the little play that is naturally present in the RDE axis leads to a non-perfect rotation, which affects the alignment of the surface (*vide infra*). In this case, this leads to the x-ray beam illuminating a polycrystalline (i.e., not single-crystalline) part of the electrode, which makes this effect easily visible. Considering that the footprint of the x-ray beam at such small incidence angles is significantly larger than the diameter of the electrode, this signal likely originates from the sides of the sample. Because of the increasing centrifugal force with increasing rotation rate, this effect is amplified at higher rotation rates.

Fortunately, in most cases, the effect on the quality of the data is rather small as most of it is captured by the background subtraction in the analysis. This can be seen in Fig. 3(b), which shows the integrated structure factors determined from the data shown in Fig. 3(a). Even though the powder rings can already be seen clearly at 1200 rpm, the intensity of the CTR is barely affected, leading to a similar signal as measured at 300 and 600 rpm. Only at 1800 rpm, the powder signal has become so strong that the CTR signal deteriorates significantly.

Several important lessons are to be learned from the data shown in Fig. 3. Obviously, an RDE rotor that provides the most perfect rotation, i.e., exhibits the least amount of play in the axis, leads to the most constant alignment position and, thus, the highest quality data. For any rotor, finding the upper limit for obtaining a stable rotation (here around 1200 rpm) by performing experiments with variable rotation rates is crucial for obtaining meaningful data for quantitative analysis. However, it should be noted that the situation shown here is a worst-case scenario. For the different measurements, the same sample alignment positions were used, which were determined at a rotation rate of 600 rpm. As the integrated angular range is rather small and the RDE rotation, albeit not perfect, is rather reproducible, better results can be obtained by performing the alignment at the rotation rate used for the experiment. This also means that, if several angular ranges are measured, the optimal alignment should be determined for these ranges individually. In practice, we found it to be easiest to first perform the overall (rough) alignment, then determine the angular ranges that are of interest, and finally fine-tune the alignment for those angular ranges. Typically, we found that, between the different angular ranges, the tilt angles are the same and the optimum sample height changes by less than 2 μm.

For a detailed structural analysis, the obtained data should also be analyzed in a quantitative manner. Figure 4 shows, for Pt(111) and Pt(100) at reducing potentials, that such an analysis is feasible [Figs. 4(a) and 4(b), respectively]. The corresponding fit parameter values are provided in the supplementary material. For Pt(111) we observe, matching previous results, that the surface structure only deviates marginally from a bulk-terminated surface (the topmost layer has a small outward relaxation and a slightly increased Debye–Waller factor).[17] For Pt(100), the CTR intensity at the surface-sensitive anti-Bragg positions is much lower than that of the bulk-terminated surface, indicating a higher surface roughness. By fitting a structural model to the data, we determine an adatom coverage of 0.17 monolayer (ML) while the underlying layers are fully occupied. This result can be understood from the preparation of the Pt(100) sample, as after flame-annealing it was cooled down in an Ar atmosphere, which is known to lead to the formation of a hexagonal surface reconstruction. This reconstruction contains 0.21 ML additional Pt atoms in the topmost layer compared to bulk-terminated Pt(100). If the reconstruction is lifted while the sample is at a low (e.g., room) temperature, (most of) these additional atoms will form adatom islands, which we observe in the CTR signal.

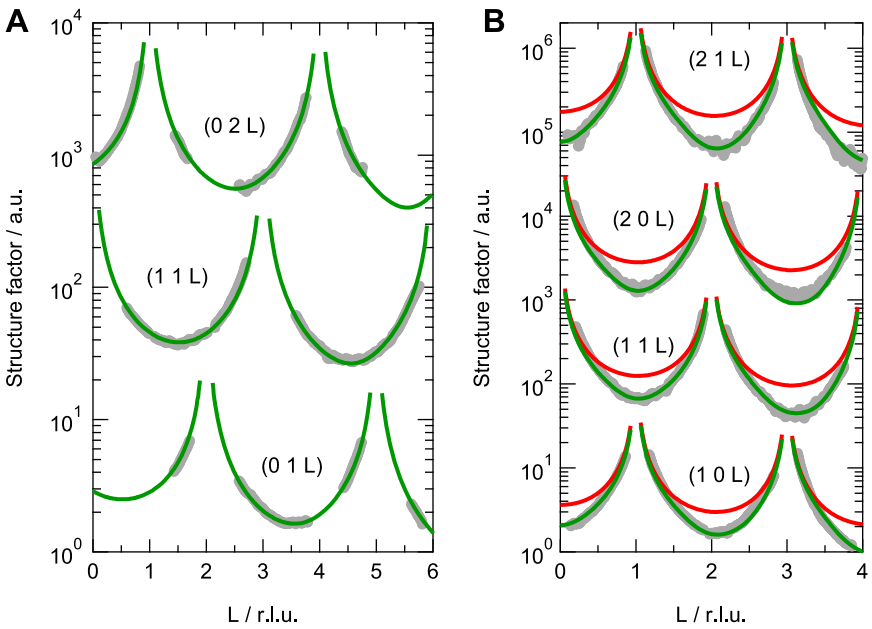

FIG. 4. Quantitative analysis: (a) (0 1), (1 1), and (0 2) CTRs of Pt(111) measured at a sample potential of 0.65 V vs RHE (gray). The green curves are the fits to the data, indicating an almost ideally bulk-terminated surface. (b) (1 0), (1 1), (2 0), and (2 1) CTRs of Pt(100) measured at a sample potential of 0.6 V vs RHE. The red curves indicate the expected signal for a bulk-terminated surface, showing strong deviations from the data in the anti-Bragg positions. The green curves include 0.17 ML of adatoms (islands) originating from the lifting of the reconstruction. The data are vertically offset for clarity.

B. Potentiodynamic measurements

Studies in electrocatalysis typically employ potential scan rates in the order of 1–100 mV s^{-1}. Relative to this, the movement of the diffractometer motors necessary to record the (HE-)SXRD signal is typically rather slow. One way to acquire data on the timescale of the electrochemical experiment is by following a single reflection as a function of potential, the so-called x-ray cyclic voltammetry (XCV).[3] Similar measurements can also be performed with the RDE setup as shown in Fig. 5. Figure 5(a) shows a crop of a single detector image from an XCV experiment, in which the sample potential was continuously cycled between 0.06 and 1.2 V vs RHE with a scan rate of 10 mV s^{-1}. The RDE rotation rate was 600 rpm, and a detector image was stored every 60 rotations, i.e., every 6 s. Therefore, the potential resolution is 60 mV. A very small angular range of only 1° is used, leading to an exposure time of 16.7 ms per image. The area within the black rectangle was background subtracted (blue rectangle) and integrated, leading to the data shown in Fig. 5(b). Here, it is clear that the intensity decreases at potentials above ~1 V vs RHE, which is known to be due to the surface oxidation that occurs via the so-called place-exchange mechanism.[17–23] Upon reduction, the surface does not fully recover to the atomically flat Pt(111) structure,[24] which explains the gradual decrease in the overall intensity with increasing cycle number.

Generally speaking, one should consider RDE measurements not the most effective for standard XCV measurements. The reason for this is that relevant data are only measured during a very small part of the rotation, here 1°, i.e., less than 0.3% of the time. Note that this ratio is independent of the employed rotation rate. However, the RDE does add a lot of flexibility to the measurement. First of all, it is very easy to tune the size of the angular integration window and thereby determine how much data is collected. In an extreme case, one could follow several surface-sensitive reflections that are separated in reciprocal space, in the case of a (111) sample, for example, around (1 1 1.5) and (1 0 2.5), in a single experiment. As XCV measurements are typically used to resolve the kinetics of structural changes rather than for a detailed quantitative structural analysis, they are less affected by the rotation rate/alignment issues described earlier.

Full CTR measurements are normally rather slow because of the diffractometer motor movements involved in such measurements. With the RDE, however, the measurement time becomes independent of the diffractometer motors and one could, in principle, do fast measurements by simply increasing the XCV angular integration window. For example, a single 10° measurement at 600 rpm takes less than 3 ms, with a repetition rate of 10 Hz (excluding symmetry equivalent CTRs). Unfortunately, in this situation, the signal will disappear in the background noise. The reason for this is that the signal intensity only depends on the exposure time at a specific angular position (when the Bragg condition is fulfilled), whereas the background scales with the total exposure time. Therefore, by increasing the angular integration window, the signal-to-noise ratio decreases compared to the data shown in Fig. 5(a). Instead of recording large sets of data with short exposure times (see Sec. II), we adopted a much simpler strategy, which can be used in case only reversible structural changes are expected. Rather than using very fast data acquisition, we employed a second detector trigger, which was connected to the sample potential. When scanning the sample potential, we now obtain integrated detector images within specific potential windows with a width of 200 mV. As those individual images have a rather low intensity, several potential sweeps are performed and summed during data processing. Figure 6(a) shows the (summed) detector images resulting from such an experiment, performed at 100, 600, and 1800 rpm. As before, the total exposure time is the same across the different images. The potential scan rate was 50 mV s^{-1}, and 10 consecutive potential cycles were performed. Figure 6(b) shows the integrated CTR profiles as a function of potential (measured at 600 rpm) as well as rotation rate. Like before, the signal deteriorates at 1800 rpm due to the sample alignment,

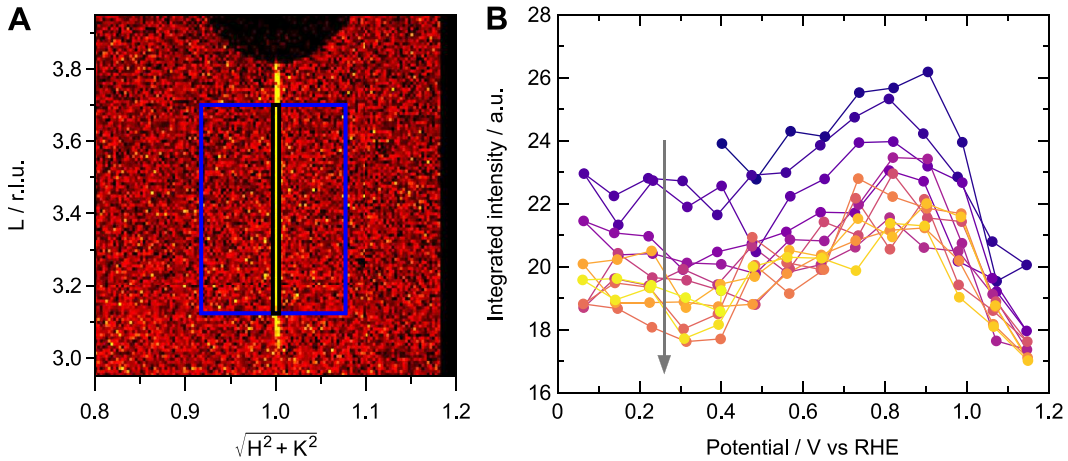

FIG. 5. Fast potentiodynamic measurements: (a) Crop of an image from the sequence of fast potentiodynamic measurements. The blue rectangle indicates the area used for background subtraction, and the black area indicates the integrated area. (b) Integrated intensity as a function of sample potential during the potential sweep. The colors indicate, from blue to yellow, the order in which the data were obtained. The decreasing intensity at potentials above 1 V matches the onset of the surface oxidation by place-exchange. Consequently, the surface roughens, leading to a decreasing intensity at the lower potentials with increasing potential cycling as indicated by the arrow.

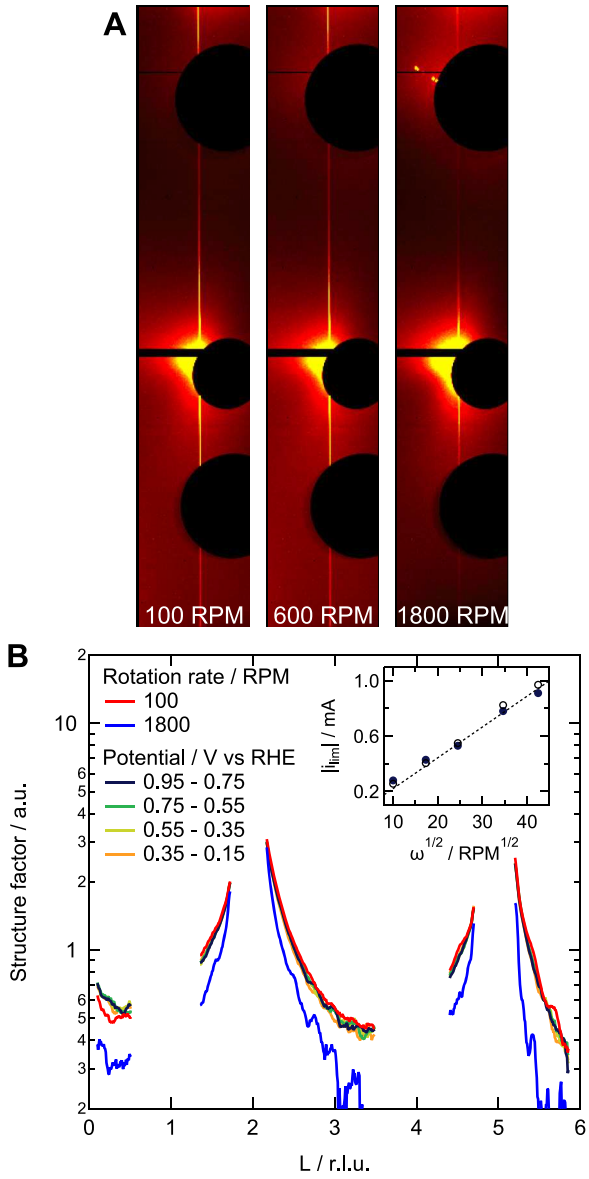

FIG. 6. Slow potentiodynamic measurements: (a) crops of the detector images showing the (0 1) CTR of Pt(111) as a function of the rotation rate, measured during a potential sweep. The color scale is the same in all images. (b) Structure factors determined from the images shown in (a) and as a function of potential (at 600 rpm) and rotation rate. The inset shows the diffusion limited ORR current as a function of the rotation rate with the x-ray beam "on" (open symbols) and "off" (filled symbols).

although here that is a bit more difficult to recognize as no (strong) powder rings appear.

These measurements were performed in an electrolyte that was saturated with O_2, which means that the oxygen reduction reaction (ORR) is taking place at all shown potentials, apart from 0.95 V. The diffusion-limited current (i_{lim}) for ORR as a function of rotation rate with the x-ray beam "on" (open symbols) and "off" (filled symbols) is shown in the inset of Fig. 6(b). The observation that the Pt(111) surface structure remains unaffected during ORR matches the XCV results obtained under static conditions by Drnec *et al.*[25] Compared to those experiments, however, the advantage of the RDE measurements is that they can be performed at higher catalytic conversion rates as i_{lim} at 600 rpm is more than 20 times larger than during the XCV measurement. Furthermore, as i_{lim} depends on the square root of the rotation rate [see inset of Fig. 6(b)] rather than the time (under static conditions), full CTRs can be measured while maintaining steady-state electrocatalytic conditions at high current densities.

IV. SUMMARY AND OUTLOOK

Structural characterization of electrode surfaces under operando electrochemical conditions is important to understand electrocatalytic reactions at a fundamental level. When employing single-crystalline model electrodes, the rotating disk electrode is the most used technique to control mass transport within the electrolyte in a well-defined manner. High-energy surface x-ray diffraction also requires an in-plane rotation of the sample, albeit typically at much smaller angular velocities as the entire diffractometer is involved in the movement. Here, we present a novel setup for combined RDE and HE-SXRD measurements, demonstrating that CTR data can readily be obtained at rotation rates of 1200 rpm. This method can also be applied at lower photon energies using a 2D detector, large enough to cover a suitable angular range. Although this would allow for very fast measurements, in practice, one becomes quickly limited by the signal-to-noise ratio. Luckily, this situation will improve with the development of new generations of synchrotrons and x-ray detectors. As a proof of principle, we have showcased several measurement schemes for electrochemical experiments, both under potentiostatic as well as potentiodynamic conditions. The method can also be applied to textured polycrystalline planar electrodes. Furthermore, it is important to realize that the general idea of a setup where only the sample rotates (rather than the entire setup) is not only of interest for electrochemical experiments but also for other HE-SXRD experiments such as in heterogeneous catalysis. Depending on the application, one can probably work with lower rotation rates and, as the electrical connection to the sample is less crucial, use a simpler but better controlled sample positioning system. This would avoid the alignment issues we observed for the highest rotation rates, while still benefiting from the advantages of a much faster sample rotation than what can typically be obtained using the diffractometer motors. With an upgraded, more stable RDE setup, the full angular range will become accessible. Finally, as the RDE ensures that all angular positions are always within reach, the flexibility in terms of the experimental setup, e.g., regarding components placed at the height of the sample surface or placement of connecting cables, increases drastically.

SUPPLEMENTARY MATERIAL

See the supplementary material for parameter values for the CTR fits in Fig. 4.

ACKNOWLEDGMENTS

We acknowledge DESY (Hamburg, Germany), a member of the Helmholtz Association HGF, for the provision of experimental facilities. Parts of this research were carried out at PETRA III, and beamtime was allocated for Proposal Nos. I-20190341 and I-20200593. We thank Simon Geile for his assistance in constructing the setup. We acknowledge financial support from the German Federal Ministry of Education and Research (BMBF Project Nos. 05K2016-HEXCHEM and 05K19WE1-CIXenergy). The authors acknowledge additional support from the Bavarian Ministry of Economic Affairs, Regional Development and Energy and the Deutsche Forschungsgemeinschaft (DFG) via the Collaborative Research Centre [Grant No. SFB 1452 (Catalysis at Liquid Interfaces, Project No. 431791331)], the Research Unit [Grant No. FOR 1878 (Functional Molecular Structures on Complex Oxide Surfaces, Project No. 214951840)], and further projects (Grant Nos. 431733372 and 453560721).

AUTHOR DECLARATIONS

Conflict of Interest

The authors have no conflicts to disclose.

Author Contributions

Leon Jacobse: Conceptualization (equal); Data curation (lead); Formal analysis (lead); Investigation (lead); Software (lead); Validation (lead); Visualization (lead); Writing-original-draft (lead); Writing-review-editing (lead). **Ralf Schuster:** Formal analysis (supporting); Investigation (equal); Visualization (supporting); Writing-review-editing (equal). **Johannes Pfrommer:** Conceptualization (supporting); Investigation (equal); Methodology (equal). **Xin Deng:** Investigation (equal); Writing-review-editing (equal). **Silvan Dolling:** Methodology (supporting). **Tim Weber:** Investigation (equal); Writing-review-editing (equal). **Olof Gutowski:** Investigation (equal); Methodology (equal); Resources (equal); Writing-review-editing (equal). **Ann-Christin Dippel:** Resources (equal); Writing-review-editing (equal). **Olaf Brummel:** Supervision (equal); Writing-review-editing (equal). **Yaroslava Lykhach:** Supervision (equal); Writing-review-editing (equal). **Herbert Over:** Conceptualization (equal); Funding acquisition (equal); Project administration (equal); Supervision (equal); Writing-review-editing (equal). **Jörg Libuda:** Project administration (equal); Supervision (equal); Writing-review-editing (equal). **Vedran Vonk:** Conceptualization (equal); Funding acquisition (equal); Investigation (equal); Method-ology (equal); Supervision (equal); Writing-review-editing (equal). **Andreas Stierle:** Conceptualization (lead); Funding acquisition (equal); Investigation (equal); Methodology (equal); Supervision (equal); Writing-review-editing (equal).

DATA AVAILABILITY

The data that support the findings of this study are available from the corresponding author upon reasonable request.

REFERENCES

[1] M. T. M. Koper, Nanoscale **3**, 2054 (2011).
[2] J. Gustafson, M. Shipilin, C. Zhang, A. Stierle, U. Hejral, U. Ruett, O. Gutowski, P. A. Carlsson, M. Skoglundh, and E. Lundgren, Science **343**, 758 (2014).
[3] G. S. Harlow, E. Lundgren, and M. Escudero-Escribano, Curr. Opin. Electrochem. **23**, 162 (2020).
[4] U. Hejral, M. Shipilin, J. Gustafson, A. Stierle, and E. Lundgren, J. Phys.: Condens. Matter **33**, 073001 (2020).
[5] U. Hejral, P. Müller, M. Shipilin, J. Gustafson, D. Franz, R. Shayduk, U. Rütt, C. Zhang, L. R. Merte, E. Lundgren, V. Vonk, and A. Stierle, Phys. Rev. B **96**, 195433 (2017).
[6] A. J. Bard and L. R. Faulkner, *Electrochemical Methods: Fundamentals and Applications*, 2nd ed. (John Wiley & Sons, Inc., 2001), p. 864.
[7] T. Weber, J. Pfrommer, M. J. S. Abb, B. Herd, O. Khalid, M. Rohnke, P. H. Lakner, J. Evertsson, S. Volkov, F. Bertram, R. Znaiguia, F. Carlà, V. Vonk, E. Lundgren, A. Stierle, and H. Over, ACS Catal. **9**, 6530 (2019).
[8] T. Weber, V. Vonk, M. J. S. Abb, J. Evertsson, M. Sandroni, J. Drnec, A. Stierle, E. Lundgren, and H. Over, J. Phys. Chem. Lett. **11**, 9057 (2020).
[9] T. Weber, V. Vonk, D. Escalera-López, G. Abbondanza, A. Larsson, V. Koller, M. J. S. Abb, Z. Hegedüs, T. Bäcker, U. Lienert, G. S. Harlow, A. Stierle, S. Cherevko, E. Lundgren, and H. Over, ACS Catal. **11**, 12651 (2021).
[10] A. Goryachev, F. Carlà, J. Drnec, W. G. Onderwaater, R. Felici, P. P. T. Krause, A. H. Wonders, E. J. M. Hensen, and J. P. Hofmann, ChemistrySelect **1**, 1104 (2016).
[11] F. Reikowski, F. Maroun, I. Pacheco, T. Wiegmann, P. Allongue, J. Stettner, and O. M. Magnussen, ACS Catal. **9**, 3811 (2019).
[12] M. L. Foresti, A. Pozzi, M. Innocenti, G. Pezzatini, F. Loglio, E. Salvietti, A. Giusti, F. D'Anca, R. Felici, and F. Borgatti, Electrochim. Acta **51**, 5532 (2006).
[13] R. Shayduk, V. Vonk, B. Arndt, D. Franz, J. Strempfer, S. Francoual, T. F. Keller, T. Spitzbart, and A. Stierle, Appl. Phys. Lett. **109**, 043107 (2016).
[14] See https://confluence.desy.de/display/PILC for extensive PiLC documentation; accessed 3 February 2022.
[15] N. Schell, A. King, F. Beckmann, T. Fischer, M. Müller, and A. Schreyer, Mater. Sci. Forum **772**, 57 (2014).
[16] J. M. Orts, R. Gómez, J. M. Feliu, A. Aldaz, and J. Clavilier, J. Phys. Chem. **100**, 2334 (1996).
[17] L. Jacobse, V. Vonk, I. T. McCrum, C. Seitz, M. T. M. Koper, M. J. Rost, and A. Stierle, Electrochim. Acta **407**, 139881 (2022).
[18] H. You, D. J. Zurawski, Z. Nagy, and R. M. Yonco, J. Chem. Phys. **100**, 4699 (1994).
[19] I. M. Tidswell, N. M. Markovic, and P. N. Ross, J. Electroanal. Chem. **376**, 119 (1994).
[20] Y. Liu, A. Barbour, V. Komanicky, and H. You, J. Phys. Chem. C **120**, 16174 (2016).
[21] J. Drnec, M. Ruge, F. Reikowski, B. Rahn, F. Carlà, R. Felici, J. Stettner, O. M. Magnussen, and D. A. Harrington, Electrochim. Acta **224**, 220 (2017).
[22] M. Ruge, J. Drnec, B. Rahn, F. Reikowski, D. A. Harrington, F. Carlà, R. Felici, J. Stettner, and O. M. Magnussen, J. Electrochem. Soc. **164**, H608 (2017).
[23] T. Fuchs, J. Drnec, F. Calle-Vallejo, N. Stubb, D. J. Sandbeck, M. Ruge, S. Cherevko, D. A. Harrington, and O. M. Magnussen, Nat. Catal. **3**, 754-761 (2020).
[24] L. Jacobse, Y.-F. Huang, M. T. M. Koper, and M. J. Rost, Nat. Mater. **17**, 277 (2018).
[25] J. Drnec, D. A. Harrington, and O. M. Magnussen, Curr. Opin. Electrochem. **4**, 69 (2017).